Molecular Biology of the Cell
Vol. 9, 3227–3239, November 1998

Contribution of the GTPase Domain to the Subcellular Localization of Dynamin in the Nematode *Caenorhabditis elegans*

Arnaud M. Labrousse, Dixie-Lee Shurland, and Alexander M. van der Bliek*

Department of Biological Chemistry, University of California Los Angeles School of Medicine, Los Angeles, California 90095

Submitted April 14, 1998; Accepted August 17, 1998
Monitoring Editor: Peter Walter

Caenorhabditis elegans dynamin is expressed at high levels in neurons and at lower levels in other cell types, consistent with the important role that dynamin plays in the recycling of synaptic vesicles. Indirect immunofluorescence showed that dynamin is concentrated along the dorsal and ventral nerve cords and in the synapse-rich nerve ring. Green fluorescent protein (GFP) fused to the N terminus of dynamin is localized to synapse-rich regions. Furthermore, this chimera was detected along the apical membrane of intestinal cells, in spermathecae, and in coelomocytes. Dynamin localization was not affected by disrupting axonal transport of synaptic vesicles in the *unc-104* (kinesin) mutant. To investigate the alternative mechanisms that dynamin might use for translocation to the synapse, we systematically tested the localization of different protein domains by fusion to GFP. Localization of each chimera was measured in one specific neuron, the ALM. The GTPase, a middle domain, and the putative coiled coil each contribute to synaptic localization. Surprisingly, the pleckstrin homology domain and the proline-rich domain, which are known to bind to coated-pit constituents, did not contribute to synaptic localization. The GFP-GTPase chimera was most strongly localized, although the GTPase domain has no known interactions with proteins other than with dynamin itself. Our results suggest that different dynamin domains contribute to axonal transport and the sequestration of a pool of dynamin molecules in synaptic cytosol.

INTRODUCTION

Dynamin is a 100-kDa GTPase, required for clathrin-mediated endocytosis (De Camilli *et al.*, 1995; Schmid, 1997; Urrutia *et al.*, 1997). Dynamin assembles into a multimeric spiral at the neck of budding vesicles (Takei *et al.*, 1995). Presumably, constriction of the dynamin spiral, driven by GTP hydrolysis, pinches vesicles off from the plasma membrane. This view is supported by a wealth of biochemical, cell culture, and genetic data. The link with endocytosis was made with the discovery that *Drosophila shibire* defects were caused by mutations in the dynamin gene (Chen *et al.*, 1991; van der Bliek and Meyerowitz, 1991). The *shibire* mutants are rapidly paralyzed when the pool of synaptic vesicles is depleted by a temperature-sensitive block in recycling via clathrin-mediated endocytosis (Poodry and Edgar, 1979; Kessel *et al.*, 1989; Narita *et al.*, 1989). Mammalian cells transfected with a dominant dynamin mutant are similarly blocked in endocytosis (Herskovits *et al.*, 1993; van der Bliek *et al.*, 1993). Nerve termini incubated with GTP-γS show tubular invaginations coated with dynamin spirals, apparently frozen in the act of pinching off (Takei *et al.*, 1995). Purified dynamin also forms spirals and some of these spirals appear partially constricted (Hinshaw and Schmid, 1995). More recently, it was shown that brain cytosol and even purified dynamin alone form vesicles when incubated with exogenous membrane (Sweitzer and Hinshaw, 1998; Takei *et al.*, 1998). Earlier electron micrographs of *shibire* flies showed electron-dense col-

* Corresponding author. E-mail address: avan@mednet.ucla.edu

lars at the necks of budding vesicles (Kosaka and Ikeda, 1983), but their significance was appreciated only after the discovery of dynamin spirals.

We recently described a *Caenorhabditis elegans* mutant with a defect in dynamin that causes temperature-sensitive paralysis similar to *shibire* flies (Clark *et al.*, 1997). *C. elegans* appears to have a single dynamin gene, *dyn-1*, which is expressed at high levels in the nervous system. Dynamin is also highly abundant in *Drosophila* and mammalian neurons where it is concentrated at synapses, possibly reflecting the high demand on endocytosis from the recycling of synaptic vesicles (Scaife and Margolis, 1990; McPherson *et al.*, 1994; Estes *et al.*, 1996). For dynamin to function in the synapse, it must be transported from the cell body where it is synthesized along the axonal process to the synapse. Axonal transport could occur through kinesin-dependent mechanisms, which are relatively fast, or through the so-called "slow transport" mechanism, which transports other cytosolic proteins like clathrin (Terada *et al.*, 1996). Once dynamin reaches the synapse, it becomes sequestered in a cytosolic matrix (Estes *et al.*, 1996). From there it can be quickly mobilized to become associated with clathrin-coated pits at the plasma membrane. One could envisage as many as three different localization signals within dynamin: 1) a signal that delivers dynamin to the synapse, 2) a signal that helps sequester dynamin in the synaptic cytosol, or 3) signals that direct dynamin molecules to a specific site on the plasma membrane for assembly into a multimeric complex. Each step could determine where and how much vesicle recycling takes place.

Dynamin has five distinct protein domains that have the potential to contribute to varying degrees to synaptic localization. At the N terminus, the first 300 amino acids make up the GTPase domain, which is highly conserved between dynamin-related proteins, constituting a distinct subgroup within the GTPase superfamily. The second domain, which we call the middle domain, has no known function. The third domain is a pleckstrin homology (PH) domain that binds to inositol phosphates and therefore may be important for interactions between dynamin and the plasma membrane (Salim *et al.*, 1996; Artalejo *et al.*, 1997). The fourth domain is a putative coiled coil that binds to the GTPase and to the middle domain (Smirnova and van der Bliek, unpublished results). Because the putative coiled coil is likely to play a role in forming dynamin multimers, we call this segment the assembly domain. The last domain is a proline-rich domain (PRD)[1], for which coprecipitation experiments showed binding to the Src homology 3 (SH3) domains of amphiphysin (David *et al.*, 1996), Grb2 (Gout *et al.*, 1993), and dynamin associated protein 160 (DAP160) (Roos and Kelly, 1998). C-terminal deletions showed that the PRD is necessary for the localization of dynamin to clathrin-coated pits (Shpetner *et al.*, 1996; Okamoto *et al.*, 1997). However, the strong synaptic localization in neurons suggests that other factors in addition to membrane targeting signals may be equally important in determining the distribution of dynamin.

We set out to identify parts of dynamin that are necessary for synaptic localization in *C. elegans* with the assumption that targeting to clathrin-coated pits is only one of a series of steps that also includes axonal transport and sequestration in the presynaptic cytosol. Knowing the different targeting mechanisms may help our understanding of synaptic function. In the present study of dynamin localization, we found that dynamin accumulates in the synapse-rich regions of the *C. elegans* nervous system, as it does in neurons of other organisms. To identify the localization signals contained within dynamin, each of the protein domains was fused to green fluorescent protein (GFP), and their subcellular distribution was determined in single neurons. The degree of localization was quantified with a new application of confocal microscopy in which we compared the fluorescence intensity of a single synaptic patch with the fluorescence intensity of an adjacent segment of the axonal process. The action of several domains of dynamin seems necessary for the protein to be optimally transported from the cell body to the nerve ring. The GTPase domain provided the most potent localization activity, revealing a novel function for this domain.

MATERIALS AND METHODS

C. elegans Strains

Worms were grown on agar plates seeded with *Escherichia coli* strain OP50 as described (Sulston and Hodgkin, 1988). The wild-type strain was Bristol N2. The dynamin mutant *dyn-1(ky51)* was described previously (Clark *et al.*, 1997). Mutant strain *dpy-20(e1282)* was kindly provided by P.W. Sternberg (California Institute of Technology, Pasadena, CA), and *unc-104(rh126)* was kindly provided by E. Hedgecock (Johns Hopkins University, Baltimore, MD). Other strains were provided by the *Caenorhabditis* Genetics Center (University of Minnesota, Saint Paul, MN) stock center.

Microinjection Procedures and Expression Constructs

Transgenic worms were obtained by microinjecting 1 ng/μl expression construct together with marker DNA. We used 50 ng/μl plasmid pRF4, which encodes the dominant *rol-6(su1006)* marker (Mello *et al.*, 1991), or 20 ng/μl plasmid pMH86, which was used to rescue *dpy-20(e1282)* animals (Han and Sternberg, 1990), and 80 ng/μl pBluescript (Stratagene, La Jolla, CA) as carrier. The pPD series of expression vectors were kindly provided by A. Fire, J. Ahnn, G. Seydoux, and S. Xu (Carnegie Institution of Washington, Baltimore, MD). DNA fragments were recloned by standard procedures. Amplification to fuse DNA fragments or to add restriction enzyme sites was done by PCR with *Pyrococcus furiosa* DNA polymerase (Pfu)

[1] Abbreviations used: GFP, green fluorescent protein; PH, pleckstrin homology; PRD, proline-rich domain; SH3, Src homology 3.

(Stratagene). The new clones were checked by sequence analysis. Boundaries of the fragments used for making the chimeric constructs are shown in Figure 6, and primer sequences are listed in Table 1. Expression was driven by the *mec-7* gene promoter (Hamelin *et al.*, 1992) or by the *dyn-1* gene promoter. Dynamin protein domains are abbreviated as GTPase, M, A, and PRD. The individual constructs were made as follows.

First Intermediate Plasmid. GFP sequences were amplified from pPD93-65 using primers A and C, cut with *Bam*HI and *Sph*I, and cloned into the dynamin gene construct pCDG1 (Clark *et al*, 1997), cut with *Bcl*I and *Sph*I.

Second Intermediate Plasmid. GFP sequences were amplified from pPD93-65 with primers B and E, and a dynamin gene fragment was amplified from pCDG1 with primers F and G. These two PCR products were fused by reamplification with primers B and G and were cloned into pPD96-41 with *Nhe*I and *Kpn*I.

dyn-1::GFP::Dynamin. A 6.2-kb *Nco*I–*Kpn*I fragment of *mec-7::GFP::Dynamin* was recloned into the first intermediate plasmid cut with the same enzymes.

dyn-1::GFP::GTPase-M-PH-A. A 3.9-kb *Nco*I–*Kpn*I fragment from *mec-7::GFP::GTPase-M-PH-A* was recloned into the first intermediate plasmid cut with the same enzymes.

dyn-1::GTPase::GFP. A 3.9-kb *Xba*I–*Bsp*EI fragment from pCDG1 was ligated to pPD95–67 cut with *Xba*I and *Age*I.

dyn-1::GFP. A 275-bp fragment of GFP was amplified with primers AA and BB, and a 300-bp fragment of dynamin was amplified with primers CC and DD using *dyn-1::GFP::Dynamin* as template. The two fragments were fused by PCR with primers CC and BB and then cloned into *dyn-1::GFP::Dynamin* with *Cla*I and *Nco*I.

mec-7::GFP. GFP sequences were amplified from pPD93-65 using primers B and D and cloned into pPD96-41 with *Nhe*I and *Kpn*I.

mec-7::GFP::Dynamin. A 4.7-kb *Pac*I–*Kpn*I fragment from pCDG1 was cloned into the second intermediate plasmid, cut with the same enzymes.

mec-7::GFP::GTPase-M-PH-A. The assembly domain was amplified from pCDG1 with primers U and V, which introduces a stop codon at the end of the assembly domain. This 295-bp fragment was cloned into *mec-7::GFP::Dynamin* with *Hpa*I and *Kpn*I.

mec-7::GFP::GTPase. The GTPase was amplified from pCDG1 with primers H and L and then cloned into the second intermediate plasmid with *Pac*I and *Kpn*I.

mec-7::GFP::PH-A-PRD. A 3.4-kb *Bcl*I–*Kpn*I fragment from pCDG1 was recloned into *Bam*HI–*Kpn*I-cut *mec-7::GFP*. To correct the reading frame between GFP and dynamin sequences, part of GFP and the linker sequence were reamplified with primers J and K and then recloned with *Nco*I and *Bcl*I.

mec-7::GFP::M. The middle domain was amplified from pCDG1 with primers M and I and then cut with *Bcl*I and ligated into *Bam*HI-cut *mec-7::GFP*. A stop codon was introduced by ligating primer T into the *Kpn*I site.

mec-7::GFP::PH. The PH domain was amplified from pCDG1 with primers N and O and then cut with *Bcl*I and ligated to *Bam*HI-cut *mec-7::GFP*.

mec-7::GFP::A. The assembly domain was amplified from pCDG1 using primers P and Q and then cut with *Bcl*I and ligated to *Bam*HI-cut *mec-7::GFP*.

mec-7::GFP::PRD. A 69-bp sequence was amplified from pCDG1 using primers R and S and then cut with *Bcl*I and *Age*I and ligated into *dyn-1::GFP*, which had been cut with *Bam*HI and *Age*I, to make *dyn-1::GFP::PRD*. This plasmid contains a 2.8-kb *Nco*I–*Kpn*I fragment, which was recloned into *mec-7::GFP* cut with the same enzymes.

Table 1. Sequences of oligonucleotides used to make expression constructs

Name	Sequence
A	CTCAGATCTTGCTAGCGATAACAAAGATGAGTAAAGGAG
B	CTCGCTAGCGATAACAAAGATGAGTAAAGGAG
C	GCGGCATGCTAATGCATTCTGATCACTTTGTATAGTTCATCCATGC
D	GTCGGTACCTCTTATAGGATCCCTCCTTTGTATAGTTCATCCATGC
E	CTGGTTTTGCCACGACATTCCACCTCCTTTGTATAGTTCATCCAT
F	ATGGATGAACTATACAAAGGAGGTGGAATGTCGTGGCAAAACCAG
G	CGCGGTACCTCGATGAGTGTCAGATTTAG
H	GAGCATCTGAAACCAGAC
I	CGCGGTACCTCACCTGGTTTCCAAGATTCTTC
J	CCTGTTCCATGGCCAACAC
K	CGCTGATCACCTGGTTTCCTGCAGCGGCCGCGCCGATCCCTCCTTTGTATAGTTC
L	CGCGGTACCTCACTTTTGAAGACTATCACG
M	CGCTGATCACGAAGATGTTTGCTATGGAAAAGG
N	GTCTTCGTGACGAGCTGG
O	CCGCTGATCATTGTTGGGACTCATCTTCC
P	CGCCTGATCATGGAGGATACCTCGATTG
Q	GCGCTGATCACTGGTCGCCAAGGGTGCTC
R	GCGTGATCATTGGCGACCAGCCGCCGCCA
S	GGCACCGGTGAAGGTCCAGAT
T	TGAAGCTTCAGTAC
U	YGCATTTGATTGTTAACC
V	CGCGGTACCTCACTGGTCGCCAAGGGTGCTC
Y	CGCGCCCGGGATCCATGGACGCTCAAGGAGATGCC
Z	CCCGCTAGCGGTACCCCTTTTCCTCCAGCCATAAAACGATG
AA	CCACCAGGATCAGCCATGAGTAAAGGAGAAGAAC
BB	CTCGCGAAGCATTGAAGACCATAACCGAAAGTAG
CC	CGCCGATCGTTTCTTCTT
DD	GTTCTTCTCCTTTACTACTGGCTGATCCTGGTGG
EE	CCAGCACCGAGCTAGCTCCAGCGGACTGTCCTCCGAC
FF	CCGCTGGAGC TAGCTCGGTGCTGGAGAATTTTGTCG

mec-7::GFP::GTPase(K46A). A 1.1-kb fragment was amplified from *dyn-1::GFP::Dynamin* using primers A and EE. A 520-bp fragment was amplified from the same template, but with primers G and FF. The two fragments were fused by amplification with primers A and G. The fusion product was cut with *Nco*I and *Pac*I and ligated into *mec-7::GFP::GTPase* cut with the same enzymes.

mec-7::GFP::M-PH-A-PRD. A 1.5-kb *Nco*I–*Hin*dIII fragment from *mec-7::GFP::M* was cloned into the first intermediate plasmid cut with the same enzymes to give *dyn-1::GFP::M*. A 3.8-kb BspE1-*Hin*dIII fragment from *dyn-1::GFP::Dynamin* was cloned into *dyn-1::GFP::M* cut with the same enzymes. This construct was then cut with *Nco*I and *Kpn*I, and the resulting 4.9-kb fragment was ligated into *Nco*I–*Kpn*I-cut *dyn-1::GFP* to make *dyn-1::GFP::M-PH-A-PRD*. Finally, a 2.4-kb fragment was cut out of *dyn-1::GFP::M-PH-A-PRD* with *Nco*I and *Hpa*I and ligated into *mec-7::GFP::PH-A-PRD* cut with the same enzymes.

Indirect Immunofluorescence

To generate anti-dynamin antibodies, we expressed the C-terminal half of *C. elegans* dynamin in *E. coli* with the bacterial expression vector pQE30 (Qiagen, Valencia, CA). This vector adds six histidines, which we used to purify the recombinant protein by Ni-affinity chromatography. Rabbit antisera were generated by Cocalico Biologicals (Reamstown, PA) and then blot purified with a dynamin protein fragment. Anti-synaptotagmin antibodies were kindly provided by Mike Nonet (Washington University, St. Louis, MO). Secondary antibodies (Boehringer Mannheim, Indianapolis, IN) were preadsorbed with acetone-powdered *C. elegans* to remove cross-reacting antibodies (Miller and Shakes, 1995).

Immunofluorescence procedures, adapted from Finney and Ruvkun (1990), were as follows. Well-fed worms were washed by pelleting and resuspending in water and then permeabilized by three cycles of freezing and thawing in 10 ml fixative (0.2 M Na-K-phosphate, pH 7.2, 4% paraformaldehyde). After three washes in 10 ml 100 mM Tris/Cl (pH 7.5), 1 mM EDTA, 1% Triton X-100 (buffer I), the worms were resuspended in 750 μl buffer I and broken with six strokes of a Dounce homogenizer (Corning Glass, Corning, NY). The worms were then incubated for 2 h at 37°C in 10 ml 0.1 M Tris/Cl (pH 6.9), 5% β-mercaptoethanol, and 1% Triton X-100, washed three times in 10 ml buffer I, followed by 2 h at 25°C in 10 ml 10 mM DTT and 1 M borate, and again washed three times in 10 ml buffer I. The worms were then gently agitated for 1–2 h at 37°C in 3 ml 10 mg/ml collagenase, 0.1 M Tris/Cl (pH 7.5), and 1 mM $CaCl_2$, followed by three washes in PBS, 3 h at 0°C in 10 ml fixative with 10 mM EGTA, and three more washes in PBS. The worms were then incubated for 16 h at 25°C in 300 μl PBS with 1% BSA, 0.5% Triton X-100, and 0.05% NaN_3 with 3 μl primary antibody, followed by three washes in 5 ml PBS with 0.2% BSA, 0.5% Triton X-100, and 0.05% NaN_3 and incubated for 3 h at 37°C with secondary antibodies in PBS with 1% BSA, 0.5% Triton X-100, and 0.05% NaN_3. After three washes in 10 ml buffer I and one wash in 1 ml mounting buffer (Molecular Probes, Eugene, OR), the worms were resuspended in Antifade (Molecular Probes) and mounted on slides coated with a thin film of dried agarose.

Microscopy and Image Analysis

Immunofluorescence was observed with a Nikon (Garden City, NY) FXA microscope equipped with filters for rhodamine and FITC. GFP was observed with an FITC excitation filter and a wide-band emission filter (Nikon B2A) so that GFP could be distinguished from the orange-tinted autofluorescence of gut granules. Confocal images were collected with a Zeiss LSM 310 microscope (Carl Zeiss, Thornwood, NY) in series of 0.75-μm optical sections that were combined into one image with the LSM software. The average intensities within a circled area covering a synaptic patch and a boxed area of identical size along the axonal process were measured with NIH Image software. The relative fluorescence intensities were then determined with a calibration plot made by imaging a series of fluorescent beads (Microscope Image Intensity Calibration Kit, Molecular Probes) using the same contrast and intensity settings of the confocal microscope as were used for the original image. Where indicated, small aggregates of GFP were eliminated by incubating the animals for 24 h at 20°C in M9 medium with 5% DMSO. A slurry of freshly grown bacteria (*E. coli* strain OP50) was added as food.

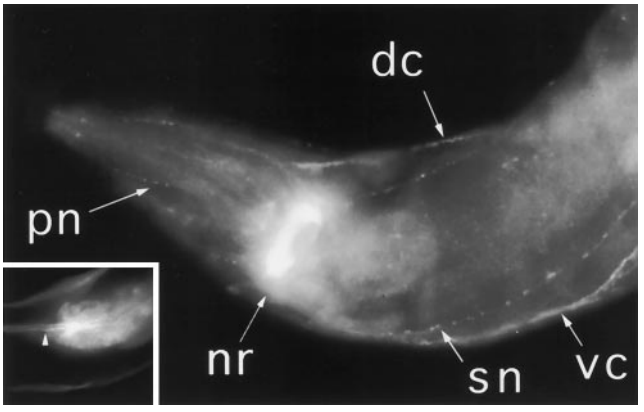

Figure 1. Endogenous dynamin detected in *C. elegans* by immunofluorescence. A wild-type (N2) animal was stained with anti-dynamin antibodies. The immunofluorescence is concentrated in the nerve ring (nr) and along ventral (vc) and dorsal (dc) nerve cords. The punctate pattern in the pharynx corresponds to pharyngeal neurons (pn). Dynamin was also detected in sublateral neurons (sn). The inset shows that dynamin accumulates along the apical surface of intestinal cells (arrowhead). In this case, the worm was broken during the permeabilization procedure, which helped unmask the specific intestinal staining.

RESULTS

Distribution of Dynamin in C. elegans Determined by Immunofluorescence

We previously showed that dynamin is expressed at high levels in the *C. elegans* nervous system using the dynamin gene promoter fused to β-galactosidase (Clark *et al.*, 1997). Here, we used immunofluorescence with an anti-dynamin antibody to investigate the subcellular distribution. We detected high levels in the nerve ring, along the ventral nerve cord, the dorsal nerve cord, and in pharyngeal neurons (Figure 1). The *C. elegans* nerve ring is a large ganglion encircling the pharynx and consists largely of axonal processes with their many synapses (White *et al.*, 1986). The nerve ring is devoid of cell bodies. Many of these cell bodies are in the head but clearly separated from the nerve ring. The concentration of fluorescence in the nerve ring indicated that dynamin was highly localized to synapse-rich regions. In some preparations, we also detected regularly spaced patches of immunofluorescence along sublateral neurons in the head (Figure 1). These patches are consistent with the location of chemical synapses detected by electron microscopy and by immunofluorescence of other synaptic proteins (Hall and Rand, personal communication; Nonet *et al.*,

1997). The localization of dynamin to chemical synapses is similar to the localization of other presynaptic proteins such as synaptotagmin (Nonet *et al.*, 1993).

Non-neuronal expression was difficult to ascertain by immunofluorescence with anti-dynamin antibodies, although our previous experiments with the *dyn-1* promoter fused to β-galactosidase also showed expression in non-neuronal cell types. In a few preparations, staining was observed along the apical surface of intestinal cells (Figure 2, inset), but more typically this staining was obscured by autofluorescence, which was also detected in control experiments omitting the primary antibody or blocking with recombinant dynamin protein (our unpublished results). Autofluorescence is largely due to the accumulation of lipofuscin in secondary lysosomes of gut granules (Clokey and Jacobson, 1986). Despite this technical difficulty, it seems likely that the dynamin gene is ubiquitously expressed, because dynamin is required for all clathrin-mediated endocytosis. As described in the next section, a more comprehensive description of dynamin localization was obtained with the *dyn-1* GFP fusions. However, the immunofluorescence results do establish the subcellular localization of endogenous dynamin in neurons, which was necessary to ensure the validity of subsequent localization experiments using GFP-chimeras.

To determine whether dynamin uses the same axonal transport mechanism as synaptic vesicles, we investigated the dynamin distribution in *unc-104* mutant animals in which synaptic vesicles stay in the neuronal cell bodies instead of being transported out to the synapses (Hall and Hedgecock, 1991). The *unc-104* gene encodes a kinesin-like protein required for axonal transport of synaptic vesicles. Synaptic vesicles can be detected by immunofluorescence with antibodies directed against synaptotagmin (Nonet *et al.*, 1993). In wild-type worms, the immunofluorescence with anti-synaptotagmin antibody is concentrated in the nerve ring and along the nerve cords in a pattern similar to that of dynamin (Figure 2, A and B, insets). In *unc-104* mutants, synaptotagmin was mislocalized to cell bodies, which were detected as fluorescent spots throughout the head (Nonet *et al.*, 1993). Synaptotagmin immunofluorescence was also concentrated in spots corresponding to neuronal cell bodies along the ventral nerve cord of *unc-104* mutant animals (Figure 2A).

In contrast to synaptotagmin, the distribution of dynamin was unaltered in *unc-104* animals, showing fluorescence concentrated in the nerve ring and evenly distributed along the ventral nerve cord (Figure 2B). This suggests that dynamin is not transported by the *unc-104* kinesin, but instead uses some other mechanism. One such transport mechanism is the so-called slow transport mechanism, which might be important for dynamin localization, because it is also used by other cytosolic proteins, such as clathrin (Terada *et al.*, 1996).

Distribution of the GFP-Dynamin Chimera in Neurons and Non-Neuronal Cells

To observe dynamin localization in vivo, we inserted GFP coding sequences between the *dyn-1* gene promoter and the dynamin protein coding sequences. Transgenic worms expressing the chimeric protein showed intense green fluorescence in the nerve ring and nerve cords in a pattern similar to that observed by immunofluorescence (Figure 3A). This pattern indicates that the chimeric protein is efficiently transported and perhaps sequestered at the synapse. The GFP-dynamin chimera enabled the detection of dynamin gene expression in non-neuronal cell types that went undetected by immunofluorescence. Autofluorescence, caused by the accumulation of lipofuscin in gut granules (Clokey and Jacobson, 1986), could be distinguished from GFP, because it has a yellow or orange tint when viewed with a broad-pass emission filter. GFP expressed in intestinal cells was made visible by the accumulation of green fluorescence at the apical surfaces (Figure 3B). This accumulation suggests a high rate of endocytosis from the intestinal lumen. We also detected dynamin along the outer membranes of the pharynx (Figure 3A), the gonadal sheath cells (Figure 3C), the spermathecae (Figure 3C), and in coelomocytes, which are scavenger cells in the *C. elegans* body cavity (Figure 3D). The expression in male animals was similar to that in hermaphrodites in their nonreproductive tissues (our unpublished results). Males also expressed GFP in cells lining the seminal vesicle and the vas deferens, and GFP forms aggregates at the point where spermatocytes bud to become spermatids before entering the seminal vesicle (our unpublished results). It is possible that these aggregates are part of the residual cytoplasmic body, which is left behind after spermatids bud from the rachis (Ward *et al.*, 1981), even though transgenes are usually not expressed in the germ line (Kelly *et al.*, 1997).

The amount of GFP-dynamin chimera as determined by Western blotting was typically between 0.2 and 0.8 times the amount of endogenous dynamin (our unpublished results). This level did not alter the temperature-sensitive paralysis of the *dyn-1 (ky51)* allele, nor did it rescue the embryonic lethal phenotype of a null allele isolated in our lab (our unpublished results). We conclude that GFP does not cause mislocalization or dominant interference, but it does interfere with the endocytic function of the attached dynamin. Similar results were obtained with GFP fused to phragmoplastin (a dynamin-like protein) in transgenic plants (Gu and Verma, 1997).

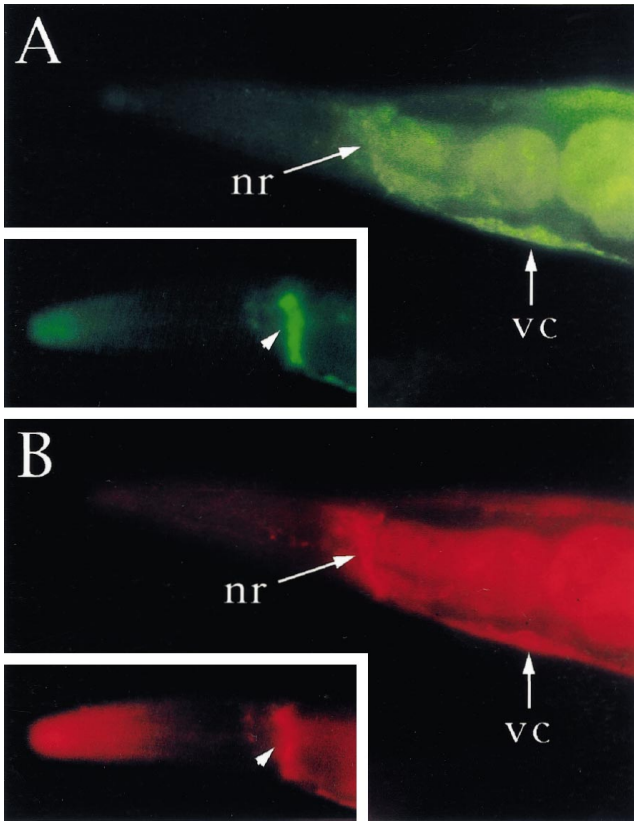

Figure 2. Dynamin localization unaffected in an *unc-104* worm. An *unc-104* mutant animal was double labeled with anti-synaptotagmin (A) and anti-dynamin antibody (B). The anti-synaptotagmin antibody showed diffuse immunofluorescence in the head and concentrated immunofluorescence in the cell bodies of the ventral nerve cord (vc), which reflects the mislocalization of synaptic vesicles in *unc-104* mutants. The anti-dynamin antibody showed immunofluorescence concentrated in the nerve ring (nr) and evenly distributed immunofluorescence along the ventral nerve cord (vc), similar to wild-type localization. The staining in the gut is mostly nonspecific, because it can also be detected in control experiments leaving out primary antibody (our unpublished results). In wild-type worms, which are shown here as a control, anti-synaptotagmin and anti-dynamin staining are both concentrated in the nerve ring (insets).

To identify parts of dynamin that conferred localization, we tested chimeric constructs in which portions of the dynamin sequence were deleted. When we tested the GFP fused to the GTPase domain, we found that this was sufficient for correct localization in neurons and intestinal cells (Figure 4C). The pattern of autofluorescence, the pattern obtained with full-length dynamin and that obtained with GFP alone are shown for comparison in Figure 4, A, B, and D. The amount GFP-GTPase localized to the nerve ring was comparable with the amounts in the surrounding neuronal cell bodies. In intestinal cells, however, localization of the GTPase domain was much more striking, showing strong fluorescence along the apical brush border.

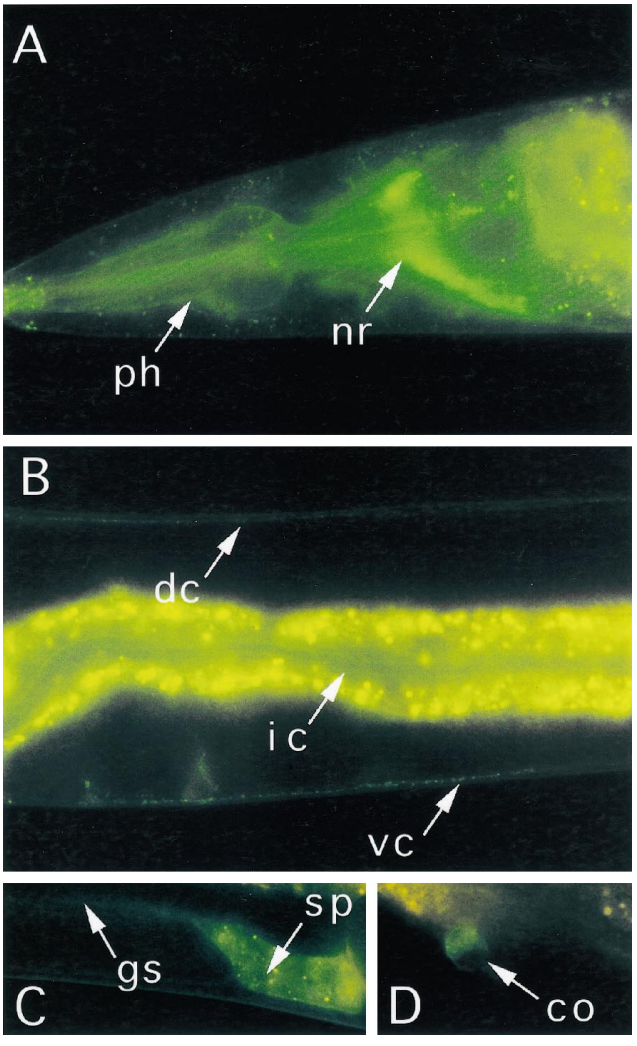

Figure 3. Localization of a GFP-dynamin chimera under control of the *dyn-1* promoter. (A) Close-up of the head region, showing that GFP-dynamin is concentrated in the nerve ring (nr). GFP-dynamin is also detected along the outside of the pharynx (ph). The yellow or orange staining of the gut is largely due to autofluorescence of gut granules. (B) Close-up of a midsection of the body, showing that the fluorescence of GFP-dynamin appears punctate along the ventral nerve cord (vc) and along the dorsal nerve cord (dc). GFP is also detectable along apical surface of the intestinal cells (ic). Some of the intestinal GFP may have been masked by the autofluorescence of gut granules (yellow-orange staining). (C) Close-up of a midsection of the body, showing fluorescence of GFP-dynamin in a spermatheca (sp) and along the gonadal sheath (gs). (D) Close-up of a midsection of the body, showing fluorescence of GFP-dynamin in a coelomocyte (co).

This result indicates that the GTPase domain is important for the localization of dynamin.

Subcellular Localization of Dynamin in ALM Neurons

Localization of specific parts of dynamin could occur if the domain in question contains a specific targeting

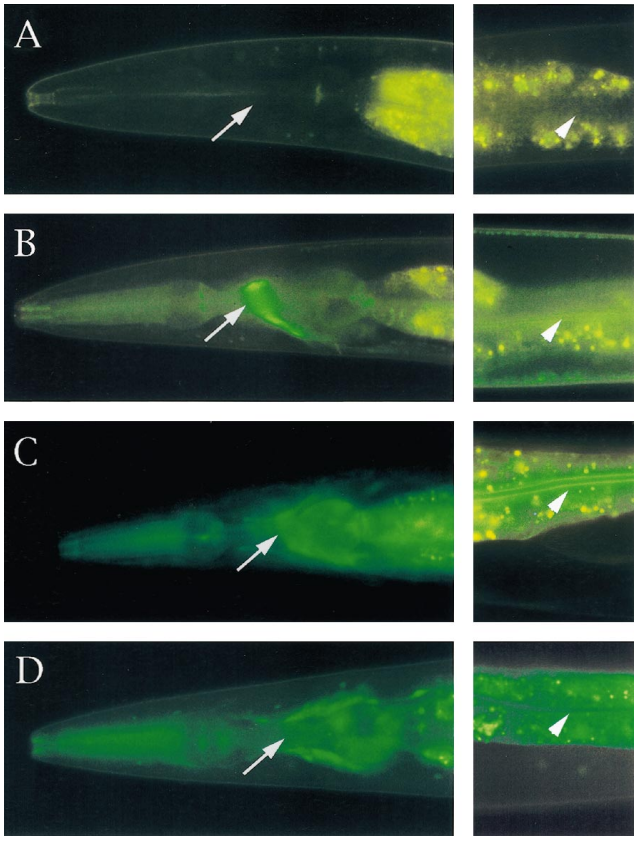

Figure 4. Localization of GFP chimeras expressed with the dynamin promoter. The left panels show the heads of transgenic animals with arrows pointing at the nerve rings. The right panels show midsections of transgenic animals with arrowheads pointing at the intestinal lining. (A) Worm with no GFP. The yellow or orange spots are gut granules, which are autofluorescent. (B) Worm containing GFP fused to full-length dynamin. The nerve ring is strongly fluorescent and there is some fluorescence detectable along the apical lining of intestinal cells (arrowheads). (C) Worm containing GFP fused to the GTPase domain. The nerve ring is still detectable, but additional diffuse fluorescence throughout the head suggests a certain degree of mislocalization. Localization to the intestinal lining was evident (arrowheads). (D) Worm containing GFP alone expressed under control of the *dyn-1* promoter. There was no detectable nerve ring fluorescence, nor was GFP detectable along the intestinal lining, although it clearly was expressed in neurons and gut cells.

signal or by association with endogenous dynamin. The latter possibility needed further consideration, because it was known that dynamin forms a multimeric complex (Tuma and Collins, 1994; Hinshaw and Schmid, 1995). Because more than one domain could participate in multimerization and targeting, it was necessary to determine the contributions of each individual dynamin domain separately. To obtain accurate information about the contributions of different domains of dynamin to synaptic localization, we generated a series of chimeras with the *mec-7* promoter fused to GFP and to the individual dynamin domains. Because the activity of the *mec-7* promoter is restricted to six touch cells (Hamelin *et al.*, 1992; Chalfie *et al.*, 1994), the promoter fusions allowed us to focus on a single pair of easily identifiable neurons, the ALMs, which have their cell bodies located just anterior of the vulva (White *et al.*, 1986). Each ALM neuron sends a process anteriorly along the lateral nerve cord ending close to the tip of the nose. A single branch enters the nerve ring and curves ventrally where it meets the AVM neuron. Electron microscopic analysis has shown presynaptic varicosities corresponding to three clusters of chemical synapses in the branches of the ALM neurons (White *et al.*, 1986).

GFP fused to full-length dynamin under the control of the *mec-7* promoter gave strong fluorescence in selected patches along the branches of the ALM neurons (Figure 5B). Similar patches were observed with GFP fused to the synaptic vesicle protein VAMP/synaptobrevin (Nonet *et al.*, 1998), although there was not enough fluorescence for quantitation (our unpublished results). These patches are likely the chemical synapses of the ALM neurons, because their size, number, and location were consistent with those detected by electron microscopy (White *et al.*, 1986). With some expression constructs, we also saw fluorescence in a few large spots in the cell body or along the axonal process in numbers that varied between animals and in locations that were clearly separated from synapses. These spots may correspond to protein aggregates, autophagosomes (Hollenbeck, 1993), or possibly axonal "traffic jams" as described in a *Drosophila* kinesin mutant (Hurd and Saxton, 1996). With one chimera (*mec-7::GFP::GTPase*) we detected punctate fluorescence throughout the ALM neurons. Exposing the worms to DMSO reduced the number of spots, which suggests that the spots were protein aggregates (our unpublished results). Fortunately, there was no indication that the spots affected the specific localization of our GFP-chimeras to the synapses.

We used confocal microscopy to quantify the degree of synaptic localization. A three-dimensional representation of the ALM neurons that were expressing the GFP chimeras was made with a series of confocal images. This series of images was converted to a single two-dimensional image, and the fluorescence intensity was determined in two selected areas, one in a synaptic patch and one in an adjacent part of the axonal process (Figure 5C). The occasional aggregates that were visible as fluorescent spots along the axonal process were avoided, because they might skew the outcome. A calibration curve, made with fluorescent beads, was used to account for the nonlinear relation between pixel values and fluorescence intensity. The degree of localization was expressed as a fluorescence ratio in which the amount of fluorescence in a synapse was divided by the amount of fluorescence in the adjacent axonal process. This approach made it possi-

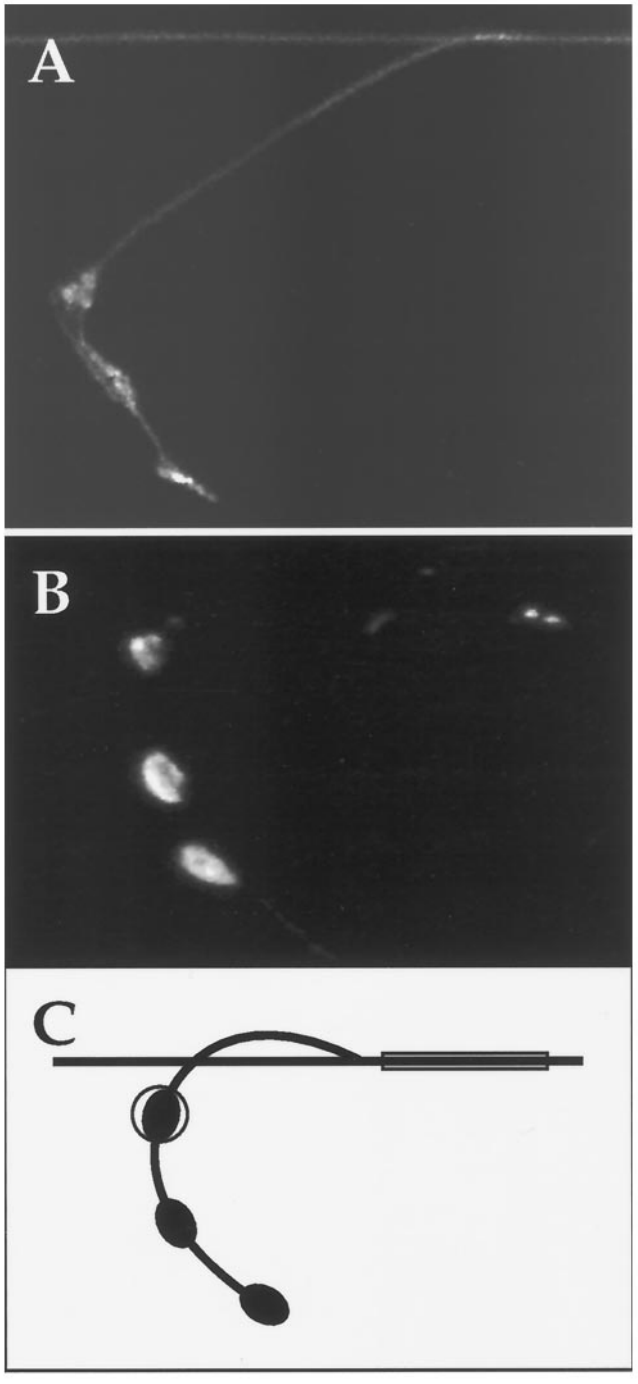

Figure 5. Green fluorescence concentrated in presynaptic varicosities of ALM neurons. (A) Distribution of GFP near the distal end of an ALM neuron. This is a close-up of the nerve ring of a transgenic worm containing the *mec-7::GFP* construct. A segment of the ALM axonal process is shown at the top. The branch, which enters the nerve ring, is shown making a curve toward the bottom. The synaptic clusters are visible as three patches of fluorescence along the branch. The image is a composite in which a stack of confocal sections was merged to visualize the curved branch of the ALM process. (B) Distribution of a GFP-dynamin chimera in part of an ALM neuron. This is a close-up of the nerve ring of a transgenic worm containing the *mec-7::GFP::Dynamin* construct. Almost all fluorescence is concentrated in the three patches corresponding to clusters of synapses. (C) Diagram of an ALM process, with a circle around one of the clusters of synapses and a box along the axonal process depicting the areas chosen to quantitate the degree of localization. The measurements were all conducted with the same surface area (200 pixels of images taken with the same magnification).

ble to quantify the degree of localization in a highly reproducible manner.

GFP alone does not accumulate in the patches, which correspond to synapses, but is instead distributed in a gradient emanating from the cell body (Figure 5A). The fluorescence intensity in the synaptic patches was very close to that in the axonal process, giving an average fluorescence ratio of 1 (Figure 6B). In marked contrast to the uniform distribution of GFP by itself, the fusion between GFP and dynamin was 17 times more concentrated in synapses than in adjacent sections of the axonal process (Figures 5B and 6B). This demonstrated that axonal transport and synaptic sequestration were not saturated by ectopic expression with the *mec-7* promoter and conversely that these mechanisms were able to localize the GFP-dynamin chimera in ALM neurons.

We tested the contribution of the individual dynamin protein domains by analyzing the distribution of GFP chimeras in ALM neurons (Figure 6). Localization, expressed as fluorescence in the synapse relative to fluorescence in the process, varied from onefold with the PH domain or PRD to sevenfold with the GTPase domain (Figure 6B). Although Western blotting verified that all chimeras were intact (our unpublished results), we could not rule out the possibility that the PH domain and PRD were misfolded or otherwise impaired by GFP. The lack of synaptic localization of these two constructs, of GFP alone, and of a GFP-β-galactosidase chimera (our unpublished results) provides a compelling argument that the localization caused by the other domains is due to a specific concentrating process. We conclude that three domains, the GTPase, the assembly, and to a lesser degree the middle, were each sufficient for specific localization to the synaptic clusters (seven-, four-, and twofold, respectively), whereas the PH domain and PRD were not (Figure 6B).

Localization of the GTPase domain in ALM neurons is consistent with the localization of chimeras expressed by the *dyn-1* promoter (Figure 4C). To test whether localization was GTP dependent, we introduced the K46A mutation, which presumably prevents GTP binding by affecting the G1 consensus motif. This mutation was previously shown to block dynamin function, but not assembly into a multimeric spiral (van der Bliek *et al.*, 1993; Warnock *et al.*, 1996). The localiza-

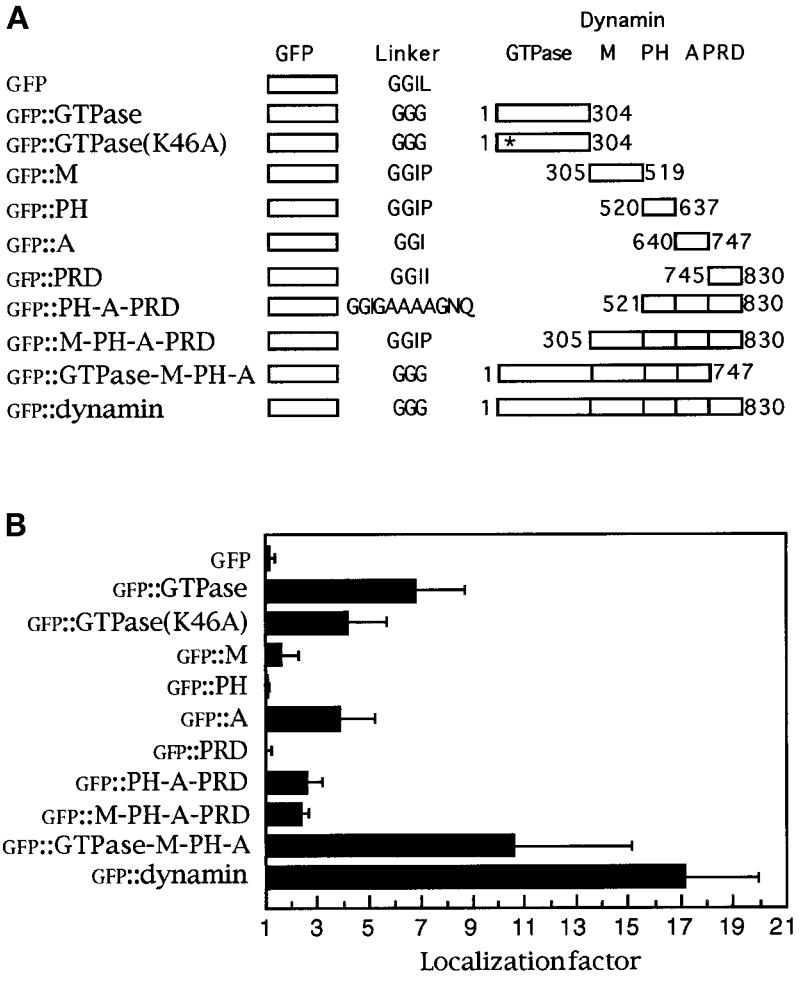

Figure 6. Localization of GFP-dynamin chimeras in ALM neurons. (A) Diagram of chimeric proteins used to study localization in ALM neurons. GFP was fused to different portions of dynamin as indicated by the amino acid numbers. The linker sequences, shown with the one-letter amino acid code, were inserted with oligonucleotides. All constructs were driven by the *mec-7* promotor. (B) Histogram showing the localization of GFP fusion proteins in ALM presynaptic varicosities relative to an adjacent section of the axonal process as indicated in Figure 5. These values were averages of 6–16 worms and are shown with the SE.

tion factor was reduced from sevenfold for the wild-type GTPase to fourfold for the K46A mutant, which suggests that GTP binding does influence localization but is not the only determinant (Figure 6B).

The finding that individual domains of dynamin were not localized to the same extent as full-length dynamin suggests that different domains act synergistically or additively, depending on whether they participate in the same process or in sequential transport events. We found that the individual localization factors were not additive when different domains were combined (Figure 6). We also found that the localization factor was influenced by the position of GFP (our unpublished results). We therefore focused on constructs containing GFP fused to the N termini of different parts of dynamin. A chimera with all but the PRD (*mec-7::GFP::GTPase-M-PH-A*) was still 11-fold more concentrated in synaptic clusters than in the axonal process (Figure 6B), consistent with nerve ring localization that could be observed with the *dyn-1* promoter (our unpublished results). Deleting the GTPase domain in *mec-7::GFP::M-PH-A-PRD* decreases the localization factor from 17-fold to 2.5-fold as expected if the GTPase domain contains a localization signal (Figure 6B).

Our findings suggest complex synergy in the localization of full-length dynamin, for example, if interactions between multiple domains were required for assembly into a multimeric complex. We conclude that three of the five domains by themselves were sufficient for localization, but that the combined action of multiple domains was necessary for maximal localization.

DISCUSSION

Neuronal Localization of Dynamin

Our experiments explored the subcellular distribution of dynamin in *C. elegans* and its underlying causes. First, the immunofluorescence and GFP chimeras showed that dynamin is concentrated in parts of the nervous system that are rich in chemical synapses.

Second, it was possible to test the contributions of the individual protein domains to localization in ALM neurons. No fewer than three of the five dynamin protein domains contribute to localization as determined by fluorescence intensity. The GTPase domain showed the highest degree of synaptic localization and was also specifically localized along the apical surface of intestinal cells. This was unexpected, because in previous experiments with transfected mammalian cells, deleting the PRD abolished localization to coated pits, and further deletions caused dynamin to lose all membrane association (Shpetner *et al.*, 1996; Okamoto *et al.*, 1997). However, our experiments did not address membrane localization, but rather localization to specialized parts of the cell, such as the presynaptic cytosol and the apical lining of intestinal cells. Therefore, our results were complementary to the results obtained by transfecting dynamin deletions into fibroblasts. Our discovery that the GTPase domain confers strong localization in situ in *C. elegans* tissue was most revealing, because it may lead to new factors that contribute to the localization process.

The strong immunofluorescence in the nerve ring and along the nerve cords most likely reflects the localization of dynamin to neuronal synapses (Figure 1). This is particularly clear for the nerve ring, which is largely devoid of cell bodies and instead consists primarily of processes connected by chemical and electrical synapses (White *et al.*, 1986). The distribution of the GFP-dynamin chimera, as seen in detail in touch cells, is also consistent with presynaptic localization, because it matches that of synaptic vesicles detected by electron microscopy (White *et al.*, 1986) and by VAMP-GFP. The distribution of *C. elegans* dynamin is similar to that in mammals and *Drosophila*, in which dynamin is highly concentrated in presynaptic cytosol, consistent with the important role that dynamin plays in synaptic vesicle recycling (Scaife and Margolis, 1990; McPherson *et al.*, 1994; Estes *et al.*, 1996). This distribution raises the question of how soluble proteins such as dynamin are transported to and become sequestered in the presynaptic cytosol.

Our analysis of *unc-104* animals indicates that dynamin is not transported together with synaptic vesicles, because synaptotagmin was clearly mislocalized, whereas dynamin was not (Figure 2). It remains possible that other kinesins transport dynamin, or that the protein is sequestered in the presynaptic varicosities following passive diffusion. However, it seems more likely that dynamin uses slow axonal transport, because the bulk of soluble proteins such as clathrin and synapsin I follow this route (Terada *et al.*, 1996).

Distribution in Non-Neuronal Cells

GFP-dynamin under control of the *dyn-1* promoter showed expression in many non-neuronal cell types (Figure 3). GFP proved to be more sensitive than immunofluorescence, because GFP-expressing worms had less background fluorescence and were not subjected to harsh permeabilization procedures. Nevertheless, the expression patterns observed with immunofluorescence and GFP both agree with previous β-galactosidase staining, showing high levels in neurons and lower levels in other cell types (Clark *et al.*, 1997). Most likely the *dyn-1* gene is ubiquitously expressed, because dynamin is essential for all clathrin-mediated endocytosis (Herskovits *et al.*, 1993; van der Bliek *et al.*, 1993), and we know of only one dynamin gene in *C. elegans* (Clark *et al.*, 1997). The *dyn-1* gene is most likely nonredundant, because a *dyn-1* null allele, recently isolated in our laboratory, is embryonic lethal (our unpublished results). We detected expression in many of the same cells that were detected previously with β-galactosidase staining, including pharyngeal muscles and intestinal cells (Clark *et al.*, 1997). However, we also detected expression in coelomocytes, spermathecae, and gonadal sheath cells. These may have been missed with β-galactosidase staining, because this procedure exhibits a threshold effect that exaggerates differences in expression levels. More importantly, the GFP-dynamin experiments also showed much more distinct subcellular localization than seen with immunofluorescence.

GFP-dynamin had a punctate distribution in coelomocytes, which might correspond to clathrin-coated pits (Figure 3D). Coelomocytes contain many coated pits, which are used to scavenge the pseudocoelomic cavity (White, 1988). A punctate distribution was also detected in spermathecae and pharyngeal muscles, where GFP-dynamin is localized to the surface facing the body cavity (Figure 3, A and C). However, it is unclear why spermathecae and pharyngeal muscles would have high rates of endocytosis. It is much easier to understand why intestinal cells have high levels of dynamin (Figure 3B). Here, GFP-dynamin was concentrated along the apical surface facing the intestinal lumen, consistent with apical microvilli supporting high rates of endocytosis to retrieve nutrients from the intestinal lumen.

Localization to the apical surface of intestinal cells was even more pronounced in transgenic animals expressing the GTPase-GFP chimera (Figure 4C). The apical lining consists of a brush border, raising the alternative possibility that the GTPase-GFP chimera is bound to a matrix component adjacent to the apical membrane, rather than binding to the membrane itself. Such sequestration may help form a pool of dynamin molecules, held in reserve to support bursts of endocytosis, similar to the pool of dynamin molecules sequestered to a cytosolic matrix component in *Drosophila* neuromuscular junctions (Estes *et al.*, 1996). Although we could not rule out localization strictly with the plasma membrane, it will be very interesting

to determine whether such alternative mechanisms exist outside the nervous system.

Localization of Individual Protein Domains

Fluorescence of the nerve ring and the intestinal lining suggests that the GTPase domain is sufficient for localization (Figure 4C). We envisage three factors that may be important for synaptic localization. First, localization might be the passive consequence of association with dynamin encoded by the endogenous *dyn-1* gene. Endogenous dynamin had to be present in all our experiments, because dynamin is essential for cell survival. Second, localization might reflect association with the axonal transport machinery. This mechanism is unlikely to occur in intestinal cells, which do localize the GTPase domain but presumably lack an intestinal equivalent of axonal transport. Third, localization might occur through passive diffusion along the axonal process followed by sequestration, either by a cytosolic matrix component or at the plasma membrane. Thus, different mechanisms may contribute to localization, depending on the specific functions of each individual domain.

Neither the PH domain nor PRD conferred synaptic localization to GFP (Figure 6B). This result was unexpected, because earlier deletion studies with mammalian cells had shown that the PRD is required to localize dynamin to coated pits (Shpetner *et al.*, 1996; Okamoto *et al.*, 1997). Coated pits contain proteins such as amphiphysin and DAP160 that bind to the dynamin PRD through their SH3 domains (David *et al.*, 1996; Roos and Kelly, 1998). These proteins may help direct dynamin to the necks of budding vesicles or control the constriction process in some other way. The PH domain also binds to a membrane component (phosphatidyl inositol 4,5-diphosphate), which may act in concert with the PRD in the final stages of localizing dynamin to coated pits (Barylko *et al.*, 1998). However, our results suggest that the interactions with the PH domain and PRD are not strong enough to sequester the chimeras in presynaptic varicosities. Evidently, other domains, such as the GTPase, middle, and assembly, contribute to synaptic localization.

Yeast two-hybrid and in vitro binding experiments with isolated dynamin fragments show three interactions between different parts of dynamin: the assembly domain binds to itself and to the GTPase and middle domains (Smirnova and van der Bliek, unpublished results). This raises the possibility that these three domains associate with endogenous dynamin and thereby piggyback to presynaptic varicosities. Such a localization mechanism seems likely for the middle and assembly domains, because these two domains showed strong binding. However, binding between the GTPase and assembly domains is relatively weak. Furthermore, the same mutation that decreases the specific localization of the GTPase domain in ALM neurons (*mec-7::GFP::GTPase(K46A)*; Figure 6B) has the opposite effect in the yeast two-hybrid system and in vitro binding experiments. The mutant GTPase domain binds more strongly to the assembly domain (our unpublished results) and was previously shown to stabilize a coassembled dynamin complex (Warnock *et al.*, 1996). This makes it unlikely that the strong localization of the wild-type GTPase domain is solely due to association with endogenous dynamin. An alternative mechanism, such as binding to a cytosolic matrix component, might contribute to the localization of the GTPase domain in neurons and intestinal cells.

Any localization signal that might be contained by the GTPase domain, and possibly by the middle and assembly domains, must be functional both in neurons and in intestinal cells. Most other GTPases, such as ras, do not contain intrinsic localization signals, but members of the rab family of small GTPases are an exception (Novick and Zerial, 1997). Each of these proteins is targeted to a specific membranous compartment by a hypervariable sequence at its C terminus (Chavrier *et al.*, 1991). For example, rab3A and rab3B are targeted to presynaptic vesicles and apical membranes of polarized epithelial cells (Weber *et al.*, 1994), which superficially resembles the targeting of the dynamin GTPase domain that we describe here. However, it seems more likely that the dynamin PH domain and PRD are responsible for the association with coated-pit constituents (phosphatidyl inositol 4,5-diphosphate and SH3 domains), whereas the GTPase domain and perhaps also some of the other dynamin domains provide a novel localization functions. Our results suggest that these localization functions are important in cells with high rates of endocytosis. The sequestration of a large pool of dynamin near the site of endocytosis enables neurons to rapidly regenerate synaptic vesicles in response to increased synaptic activity, whereas intestinal cells may also require localized dynamin to sustain high rates of endocytosis when food becomes available. Distinguishing the contributions of different dynamin domains will help unravel the localization process.

ACKNOWLEDGMENTS

We thank G. Payne and J. Vowels for valuable suggestions and comments on the manuscript. We thank C. Bargmann (University of California San Fransisco, San Fransisco, CA) for first suggesting the possible role of the GTPase in localization. We thank A. Fire, J. Ahnn, G. Seydoux, and S. Xu (Carnegie Institution of Washington) for expression vectors. We thank M. Nonet (Washington University) for the gift of anti-synaptotagmin antibodies and E. Hedgecock (Johns Hopkins University) for *unc-104* alleles. Some strains were obtained from the *Caenorhabditis* Genetics Center (University of Minnesota, St. Paul, MN). This work was supported by National Institutes of Health grant GM51866 to A.M.v.d.B. A.M.L. was sup-

ported by fellowships from the Association pour la Recherche Contre le Cancer and Fondation pour la Recherche Médicale.

REFERENCES

Artalejo, C.R., Lemmon, M.A., Schlessinger, J., and Palfrey, H.C. (1997). Specific role for the PH domain of dynamin−1 in the regulation of rapid endocytosis in adrenal chromaffin cells. EMBO J. *16*, 1565–1574.

Barylko, B., Binns, D., Lin, K.M., Atkinson, M.A., Jameson, D.M., Yin, H.L., and Albanesi, J.P. (1998). Synergistic activation of dynamin GTPase by Grb2 and phosphoinositides. J. Biol. Chem. *273*, 3791–3797.

Chalfie, M., Tu, Y., Euskirchen, G., Ward, W.W., and Prasher, D.C. (1994). Green fluorescent protein as a marker for gene expression. Science *263*, 802–805.

Chavrier, P., Gorvel, J.P., Stelzer, E., Simons, K., Gruenberg, J., and Zerial, M. (1991). Hypervariable C-terminal domain of rab proteins acts as a targeting signal. Nature *353*, 769–772.

Chen, M.S., Obar, R.A., Schroeder, C.C., Austin, T.W., Poodry, C.A., Wadsworth, S.C., and Vallee, R.B. (1991). Multiple forms of dynamin are encoded by *shibire*, a *Drosophila* gene involved in endocytosis. Nature *351*, 583–586.

Clark, S.G., Shurland, D.L., Meyerowitz, E.M., Bargmann, C.I., and van der Bliek, A.M. (1997).A dynamin GTPase mutation causes a rapid and reversible temperature-inducible locomotion defect in *C. elegans*. Proc. Natl. Acad. Sci. USA *94*, 10438–10443.

Clokey, G.V., and Jacobson, L.A. (1986). The autofluorescent "lipofuscin granules" in the intestinal cells of *Caenorhabditis elegans* are secondary lysosomes. Mech. Ageing Dev. *35*, 79–94.

David, C., McPherson, P.S., Mundigl, O., and de Camilli, P. (1996). A role of amphiphysin in synaptic vesicle endocytosis suggested by its binding to dynamin in nerve terminals. Proc. Natl. Acad. Sci. USA *93*, 331–335.

De Camilli, P., Takei, K., and McPherson, P.S. (1995). The function of dynamin in endocytosis. Curr. Opin. Neurobiol. *5*, 559–565.

Estes, P.S., Roos, J., van der Bliek, A.M., Kelly, R.B., Krishnan, K.S., and Ramaswami, M. (1996). Traffic of dynamin within individual *Drosophila* synaptic boutons relative to compartment-specific markers. J. Neurosci. *16*, 5443–5456.

Finney, M., and Ruvkun, G. (1990). The *unc-86* gene product couples cell lineage and cell identity in *C. elegans*. Cell *63*, 895–905.

Gout, I., *et al.* (1993). The GTPase dynamin binds to and is activated by a subset of SH3 domains. Cell *75*, 25–36.

Gu, X., and Verma, D.P. (1997). Dynamics of phragmoplastin in living cells during cell plate formation and uncoupling of cell elongation from the plane of cell division. Plant Cell *9*, 157–169.

Hall, D.H., and Hedgecock, E.M. (1991). Kinesin-related gene *unc-104* is required for axonal transport of synaptic vesicles in *C. elegans*. Cell *65*, 837–847.

Hamelin, M., Scott, I.M., Way, J.C., and Culotti, J.G. (1992). The mec-7 beta-tubulin gene of *Caenorhabditis elegans* is expressed primarily in the touch receptor neurons. EMBO J. *11*, 2885–2893.

Han, M., and Sternberg, P.W. (1990). *let-60*, a gene that specifies cell fates during *C. elegans* vulval induction, encodes a *ras* protein. Cell *63*, 921–931.

Herskovits, J.S., Burgess, C.C., Obar, R.A., and Vallee, R.B. (1993). Effects of mutant rat dynamin on endocytosis. J. Cell Biol. *122*, 565–578.

Hinshaw, J.E., and Schmid, S.L. (1995). Dynamin self-assembles into rings suggesting a mechanism for coated vesicle budding. Nature *374*, 190–192.

Hollenbeck, P.J. (1993). Products of endocytosis and autophagy are retrieved from axons by regulated retrograde organelle transport. J. Cell Biol. *121*, 305–315.

Hurd, D.D., and Saxton, W. (1996). Kinesin mutations cause motor neuron disease phenotypes by disrupting fast axonal transport in *Drosophila*. Genetics *144*, 1075–1085.

Kelly, W.G., Xu, S., Montgomery, M.K., and Fire, A. (1997). Distinct requirements for somatic and germline expression of a generally expressed *Caenorhabditis elegans* gene. Genetics *146*, 227–238.

Kessel, I., Holst, B.D., and Roth, T.F. (1989). Membranous intermediates in endocytosis are labile, as shown in a temperature-sensitive mutant. Proc. Natl. Acad. Sci. USA *86*, 4968–4972.

Kosaka, T., and Ikeda, K. (1983). Possible temperature-dependent blockage of synaptic vesicle recycling induced by a single gene mutation in *Drosophila*. J. Neurobiol. *14*, 207–225.

McPherson, P.S., Takei, K., Schmid, S.L., and De Camilli, P. (1994). p145, a major Grb2-binding protein in brain, is co-localized with dynamin in nerve terminals where it undergoes activity-dependent dephosphorylation. J. Biol. Chem. *269*, 30132–30139.

Mello, C.C., Kramer, J.M., Stinchcomb, D., and Ambros, V. (1991). Efficient gene transfer in *C. elegans*: extrachromosomal maintenance and integration of transforming sequences. EMBO J. *10*, 3959–3970.

Miller, D.M., and Shakes, D.C. (1995). Immunofluorescence microscopy. Methods Cell. Biol. *48*, 365–394.

Narita, K., Tsuruhara, T., Koenig, J.H., and Ikeda, K. (1989). Membrane pinch-off and reinsertion observed in living cells of *Drosophila*. J. Cell. Physiol. *141*, 383–391.

Nonet, M.L., Grundahl, K., Meyer, B.J., and Rand, J.B. (1993). Synaptic function is impaired but not eliminated in *C. elegans* mutants lacking synaptotagmin. Cell *73*, 1291–1305.

Nonet, M.L., Saifee, O., Zhao, H., Rand, J.B., and Wei, L. (1998). Synaptic transmission deficits in *Caenorhabditis elegans* synaptobrevin mutants. J. Neurosci. *18*, 70–80.

Nonet, M.L., Staunton, J.E., Kilgard, M.P., Fergestad, T., Hartwieg, E., Horvitz, H.R., Jorgensen, E.M., and Meyer, B.J. (1997). *Caenorhabditis elegans* rab-3 mutant synapses exhibit impaired function and are partially depleted of vesicles. J. Neurosci. *17*, 8061–8073.

Novick, P., and Zerial, M. (1997). The diversity of Rab proteins in vesicle transport. Curr. Opin. Cell Biol. *9*, 496–504.

Okamoto, P.M., Herskovits, J.S., and Vallee, R.B. (1997). Role of the basic, proline-rich region of dynamin in Src homology 3 domain binding and endocytosis. J. Biol. Chem. *272*, 11629–11635.

Poodry, C.A., and Edgar, L. (1979). Reversible alterations in the neuromuscular junctions of *Drosophila melanogaster* bearing a temperature-sensitive mutation, *shibire*. J. Cell Biol. *81*, 520–527.

Roos, J., and Kelly, R.B. (1998). Dap160, a neural-specific Eps15 homology and multiple SH3 domain-containing protein that interacts with *Drosophila* dynamin. J. Biol. Chem. *273*, 19108–19.

Salim, K., *et al.* (1996). Distinct specificity in the recognition of phosphoinositides by the pleckstrin homology domains of dynamin and Bruton's tyrosine kinase. EMBO J. *15*, 6241–6250.

Scaife, R., and Margolis, R.L. (1990). Biochemical and immunochemical analysis of rat brain dynamin interaction with microtubules and organelles in vivo and in vitro. J. Cell Biol. *111*, 3023–3033.

Schmid, S.L. (1997). Clathrin-coated vesicle formation and protein sorting: an integrated process. Annu. Rev. Biochem. *66*, 511–548.

Shpetner, H.S., Herskovits, J.S., and Vallee, R.B. (1996). A binding site for SH3 domains targets dynamin to coated pits. J. Biol. Chem. *271*, 13–16.

Sulston, J., and Hodgkin, J. (1988). Methods. In: The Nematode *Caenorhabditis elegans*, ed. W.B. Wood, Cold Spring Harbor, NY: Cold Spring Harbor Laboratory Press, 587–606.

Sweitzer, S.M., and Hinshaw, J.E. (1998). Dynamin undergoes a GTP-dependent conformational change causing vesiculation. Cell *93*, 1021–1029.

Takei, K., Haucke, V., Slepnev, V., Farsad, K., Salazar, M., Chen, H., and De Camilli, P. (1998). Generation of coated intermediates of clathrin-mediated endocytosis on protein-free liposomes. Cell *94*, 131–141.

Takei, K., McPherson, P.S., Schmid, S.L., and DeCamilli, P. (1995). Tubular invaginations coated by dynamin rings are induced by GTPγS in nerve terminals. Nature *374*, 186–190.

Terada, S., Nakata, T., Peterson, A.C., and Hirokawa, N. (1996). Visualization of slow axonal transport in vivo. Science *273*, 784–788.

Tuma, P.L., and Collins, C.A. (1994). Activation of dynamin GTPase is a result of positive cooperativity. J. Biol. Chem. *269*, 30842–30847.

Urrutia, R., Henley, J.R., Cook, T., and McNiven, M.A. (1997). The dynamins: redundant or distinct functions for an expanding family of related GTPases? Proc. Natl. Acad. Sci. USA *94*, 377–384.

van der Bliek, A.M., and Meyerowitz, E.M. (1991). Dynamin-like protein encoded by the *Drosophila* shibire gene associated with vesicular traffic. Nature *351*, 411–414.

van der Bliek, A.M., Redelmeier, T.E., Damke, H., Tisdale, E.J., Meyerowitz, E.M., and Schmid, S.L. (1993). Mutations in human dynamin block an intermediate stage in coated vesicle formation. J. Cell Biol. *122*, 553–563.

Ward, S., Argon, Y., and Nelson, G.A. (1981). Sperm morphogenesis in wild-type and fertilization-defective mutants of *Caenorhabditis elegans*. J. Cell Biol. *91*, 26–44.

Warnock, D.E., Hinshaw, J.E., and Schmid, S.L. (1996). Dynamin self-assembly stimulates its GTPase activity. J. Biol. Chem. *271*, 22310–22314.

Weber, E., *et al*. (1994). Expression and polarized targeting of a rab3 isoform in epithelial cells. J. Cell Biol. *125*, 583–594.

White, J. (1988). The anatomy. In: The Nematode *Caenorhabditis elegans*, ed. W.B. Wood, Cold Spring Harbor, NY: Cold Spring Harbor Laboratory Press, 81–122.

White, J., Southgate, E., Thomson, J., and Brenner, S. (1986). The structure of the nervous system of the nematode *Caenorhabditis elegans*. Philos. Trans. R. Soc. Lond. B Biol. Sci. *314*, 1–340.